Supporting Information

Unexpected Effect of an Axial Ligand Mutation in the Type 1 Copper Center in Small Laccase: Structure-Based Analyses and Engineering to Increase Reduction Potential and Activity

Jing-Xiang Wang, Avery C. Vilbert, Lucas H. Williams, Evan N. Mirts, Chang Cui, Yi Lu*

Experimental Procedures

Unless stated otherwise, all materials and reagents were purchased from either Millipore Sigma or Fisher Scientific and used without further purification.

Protein purification and spectroscopy

Mutations were introduced into WT-SLAC by site-directed mutagenesis and the mutants were expressed and purified based on the previously reported protocol.[1] The protein is stored and characterized in 50 mM 3-(N-morpholino)propanesulfonic acid (MOPS), 150 mM NaCl, pH 7.0 buffer unless specified. The resulting protein is verified by electrospray ionization mass spectroscopy (ESI-MS). The copper content of each mutant is characterized using 2,2'-biquinoline assay.[1,2] Electronic absorption spectroscopy was measured using Agilent Cary 60 UV-Vis Spectrophotometer in 50 mM MOPS, 150 mM NaCl, pH 7.0 buffer. Continuous X-band (9.42 GHz) EPR spectra were recorded on Bruker EMXplus at 77-100 K (Power: 2 mW; Modulation amplitude: 7.46 G). Samples were prepared with 250 μM protein in 50 mM MOPS 150 mM NaCl pH 7.0 buffer. Spectra were fit using EasySpin MATLAB package.[3] The extinction coefficient of type 1 copper (T1Cu) for each mutant was calculated by measuring the absorption spectra of the EPR samples, then used the double integration from the T1Cu species in the EPR spectra to quantify the amount of T1Cu in the sample, and finally compared with the measurement from WT-SLAC. The extinction coefficient of T1Cu center in WT-SLAC has been reported before to be 4400 $M^{-1}cm^{-1}$ and was used as standard.[4]

Protein crystallography and data analysis

Protein was crystallized based on the reported method[1]. Basically, crystals were grown using the hanging drop vapor-diffusion technique at room temperature (~23°C). Protein is at a concentration of 18.5 $mg \cdot ml^{-1}$ in 50 mM H_3BO_3, 0.1 M NaCl, pH 9.0 buffer. The well buffer contains 0.1 M glycine, 0.5 M NaCl, pH 9.0, and 37-40% (v/v) polyethylene glycol monomethyl ether (mPEG) 550. Each well is added with 500 μL of well buffer and protein is mixed with well buffer at a 1.5 μL:1.5 μL ratio. The crystal growth time was ca. 1-2 weeks.

X-ray diffraction data were acquired at the beamline 8.2.1 at the Advanced Light Source (ALS) of the Lawrence Berkeley National Laboratory or beamline 23-ID-B at the Advanced Photon Source (APS) of the Argonne National Laboratory. Diffraction images were integrated and processed with xia2-DIALS[5,6] in the CCP4i2[7,8]. The crystal structure was solved by molecular replacement method from the structure of S292F-SLAC (PDB: 8U8P[1]) using Phaser in the PHENIX software suite[9,10]. Refinement was performed in PHENIX and Coot[11]. The final models were evaluated using MolProbity[12] and displayed in PyMOL[13].

Redox titration

All redox titration experiments were conducted in a glovebox under N_2 atmosphere. Aliquots of protein were equilibrated in glovebox overnight prior to use. Ferricyanide stock (100 mM) and sodium dithionite stock (4 mM) was freshly prepared in the glovebox using 50 mM MOPS, 150 mM NaCl, pH 7 buffer. Internal indicator (ferricyanide) was mixed with protein in a total volume of 200 μL and a final concentration of ~1 mM indicator and 70 μM protein. The absorption spectrum was recorded using Agilent Cary 60 UV-Vis Spectrophotometer. Next, the absorption was monitored following addition of 0.5-1 μL dithionite stock solution after equilibration. The relative peak intensity at 565 nm for M298L-SLAC, 590 nm for LF-SLAC, and 580 nm for LF-M298L-SLAC was used to indicate the percentage of oxidized form proteins. The relative peak intensity at 420 nm, after subtracting the protein absorption contribution for M298L-SLAC or LF-M298L-SLAC based on their intensity at 565 nm or 580 nm, was used to indicate the percentage of oxidized form indicators after subtracting the contribution from protein. To determine the protein absorption at 420 nm, M298L-SLAC or LF-M298L-SLAC is first reduced gradually by addition of

0.5-1 μL dithionite without the presence of ferricyanide, while the decrease of peaks at 420 nm and 565 nm or 580 nm are monitored. The ratio between the decrease of the two peaks is found to be constant. This constant is used for calculating the protein absorption at 420 nm when mixed with ferricyanide. Then, the Nernst equation was applied to get the potential of T1Cu in protein with a reference of 436 mV vs. SHE for ferricyanide.

Molecular dynamics simulations

MD simulations were performed using ASH, a Python-based computational chemistry and multiscale modelling program (https://ash.readthedocs.io/en/latest/About.html) with an interface to the OpenMM library,[14] and CHARMM36 forcefield.[15] The starting model was the crystal structure of M298L-SLAC and N47S/M121L-Az (PDB: 3JT2[16]). The histidines in T1Cu center were protonated at NE2, while the histidines in trinuclear center were protonated at ND1. To keep the correct coordination geometry of the copper centers, the distances between copper and the coordinating atoms were constrained. The systems were neutralized and solvated in a cubic box with 100 mM NaCl and at least 1 nm from the protein to the edge of the box. The water was described by TIP3P model.[17] The simulation for azurin contains 6218 water molecules, while the simulation for SLAC contains 27487 water molecules.

The initial geometry was minimized for 100 steps, then gently warmed up with three successive simulations to 1 K, 10 K, and 300 K using 10, 50, 200 steps with timesteps of 0.5, 1, 4 fs. Then the box was equilibrated at 300 K and 1 bar of pressure until the volume variation was less than 1.0 nm^3 and density variation was less than 0.004 g/mL. Production NVT simulations were conducted for 1 ns under 300 K. The frequency of each state is analyzed by change point analysis on the trajectory plot.

ABTS activity assay

A fresh 50 mM solution of 2,2'-azino-bis(3-ethylbenzothiazoline-6-sulfonic acid) (ABTS) diammonium salt was prepared fresh by dissolving 54.87 mg into 2 mL 50 mM MOPS, 150 mM NaCl, pH 7 buffer. Measurements were taken under kinetic mode of Agilent 8453 UV-visible Spectroscopy at 2 s intervals in 1 mL of 50 mM MOPS, 150 mM NaCl, pH 7 buffer under 310 K and the absorbance at 420 nm from $ABTS^{+\cdot}$ was monitored. The solution was continuously stirred in aerobic conditions to ensure saturating O_2 conditions. ABTS was added in concentrations from 0.1 mM to 4 mM and background oxidation rate was measured through linear fitting. Then, 5 μM of M298L-SLAC, or 1 μM of LF-SLAC, or 1 μM of LF-M298L-SLAC was added to initiate the reaction. All experiments were measured in triplicate. The observed rate (v_{obs}) was measured by the slope of the tangent line of the kinetic curve. The initial v_{obs} values and the corresponding ABTS concentration were then fit to the Michaelis-Menten curve to obtain both k_{cat} and K_M values.

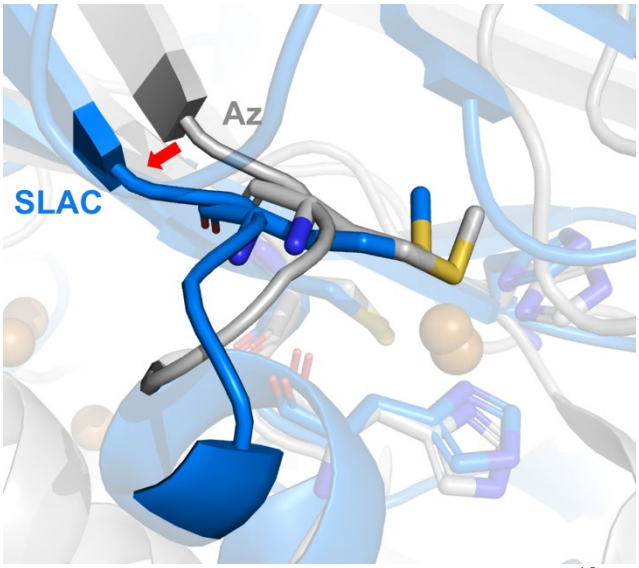

Figure S1. Structure alignment between WT-SLAC (blue, PDB: 3CG8[18]) and WT-azurin (white, PDB: 4AZU[19]). The red arrow indicates the shift of the loop that holds the axial methionine.

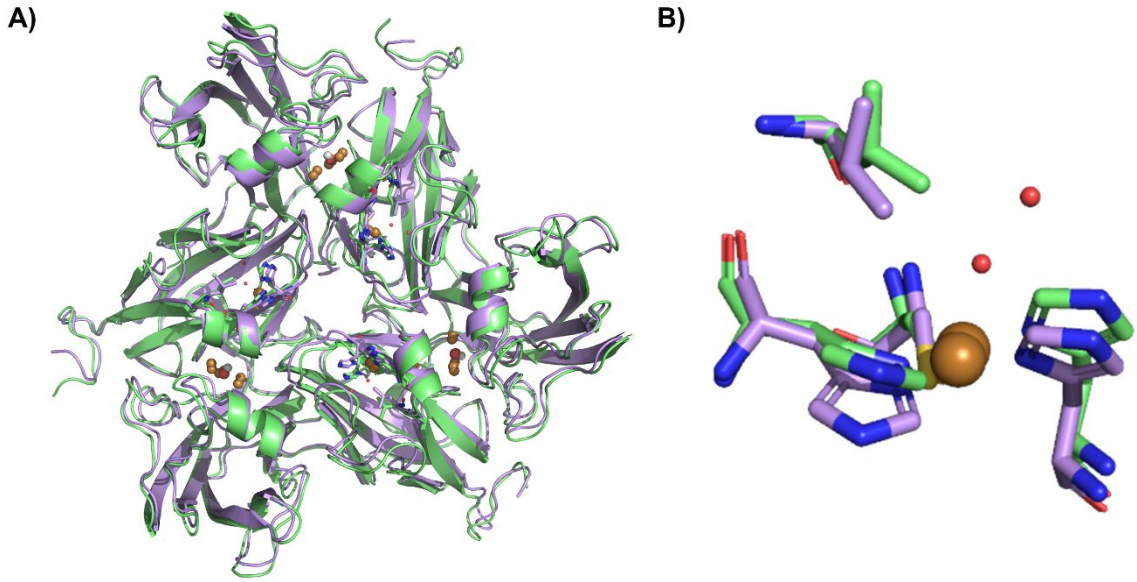

Figure S2. Structure alignment between crystal structure (purple, PDB: 9NJI) and MD simulation result (green) of M298L-SLAC. A) Overall structure; B) T1Cu site. The red spheres are the axial water molecules in the crystal structure.

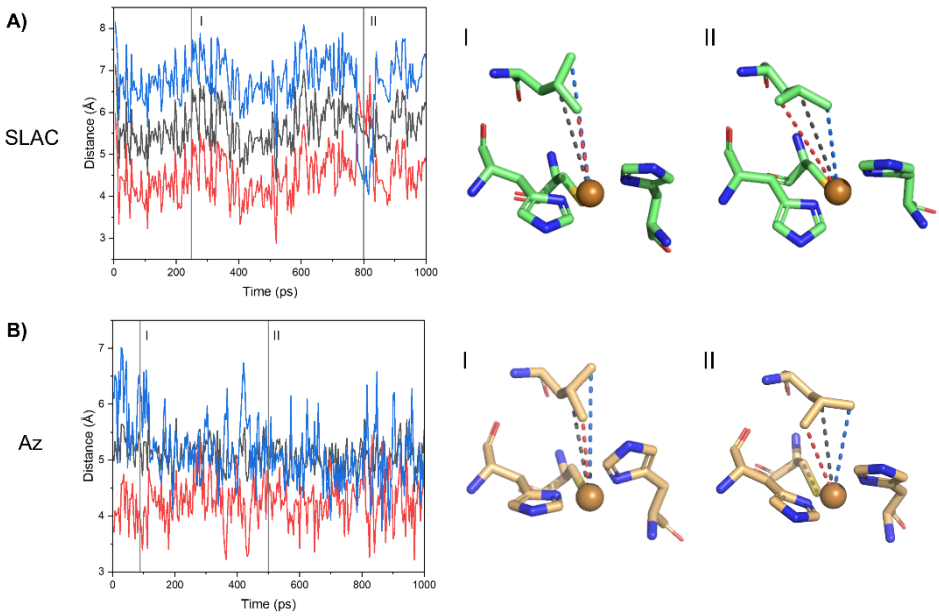

Figure S3. The distance between T1Cu and different carbon atoms in axial leucine over 1000 ps of MD simulation revealed two conformations (**I** and **II**) the axial leucine can adopt. A) SLAC; B) Az.

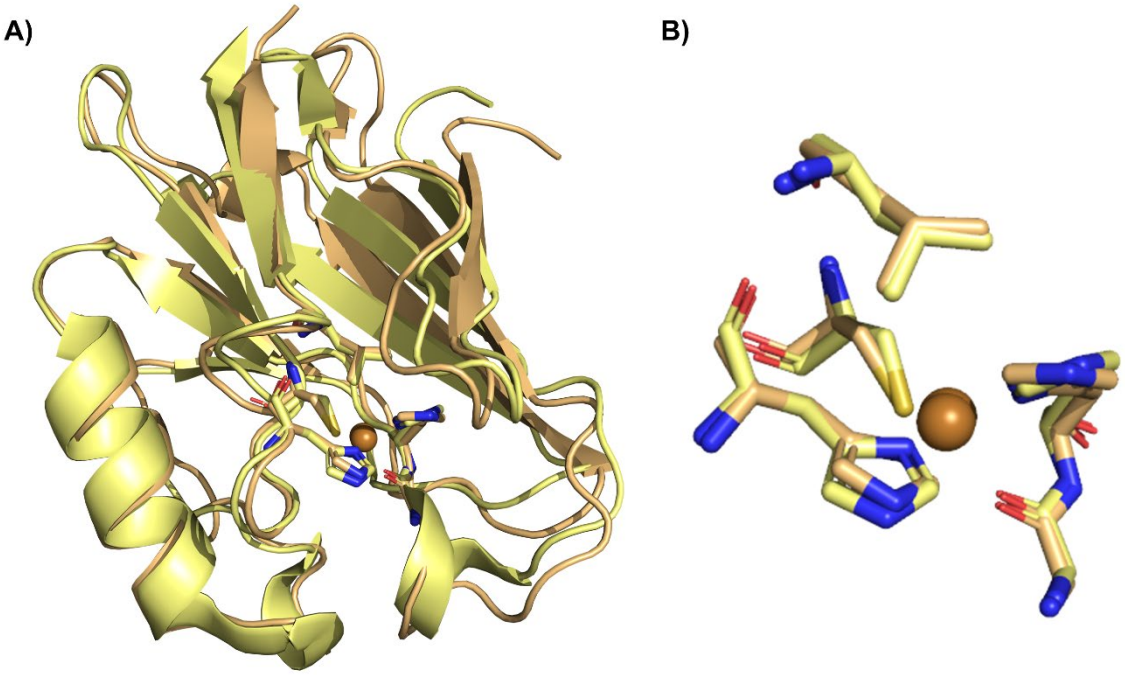

Figure S4. Structure alignment between crystal structure (yellow, PDB: 3JT2[16]) and MD simulation result (orange) of N47S/M121L-Az. A) Overall structure; B) T1Cu site.

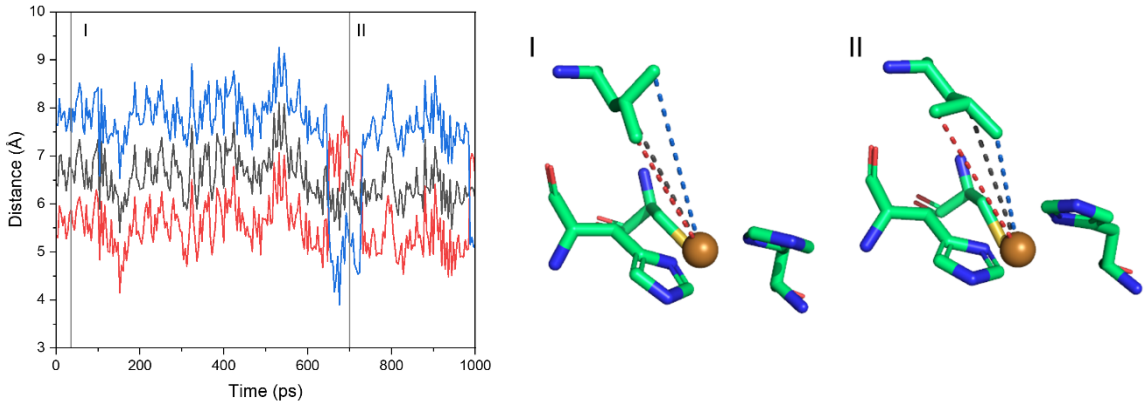

Figure S5. The distance between T1Cu and different carbon atoms in axial leucine of M298L-SLAC over 1000 ps of MD simulation with conformations **II** as the starting structure.

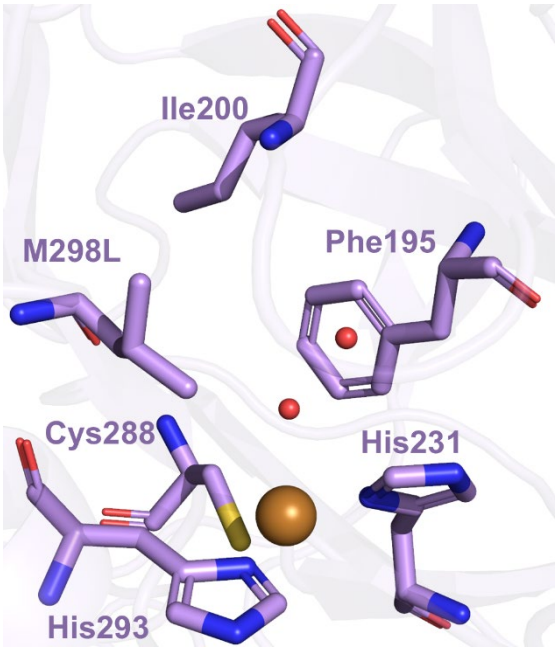

Figure S6. Position of Phe195 and Ile200 relative to the axial water molecules in the crystal structure of M298L-SLAC (PDB: 9NJI).

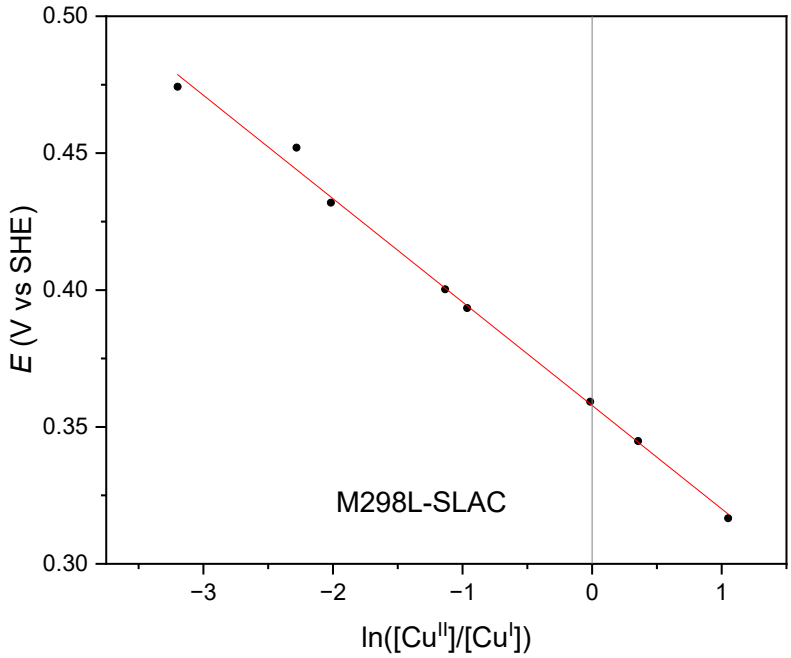

Figure S7. Redox titration of M298L-SLAC in 50 mM MOPS 150 mM NaCl pH 7 buffer. (R^2 = 0.996)

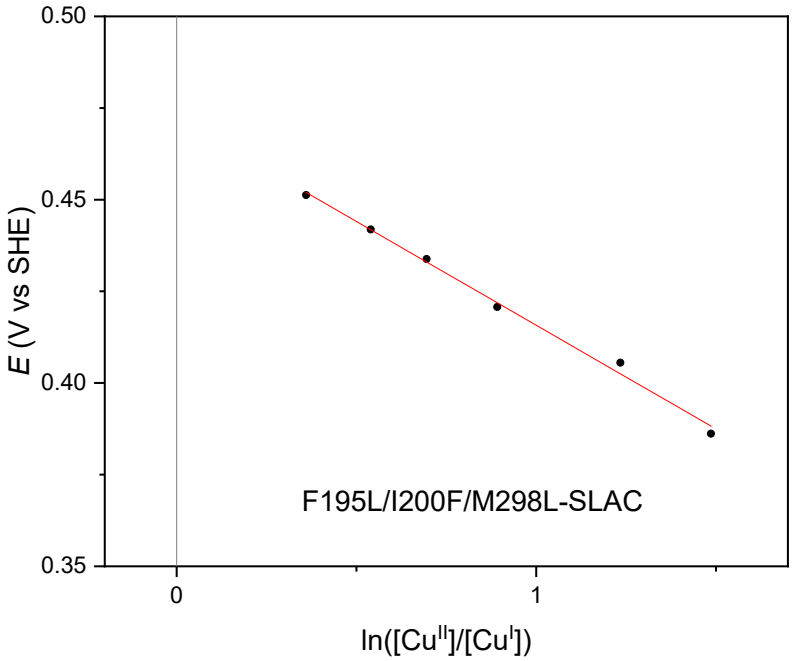

Figure S8. Redox titration of F195L/I200F/M298L-SLAC in 50 mM MOPS 150 mM NaCl pH 7 buffer. (R^2 = 0.995)

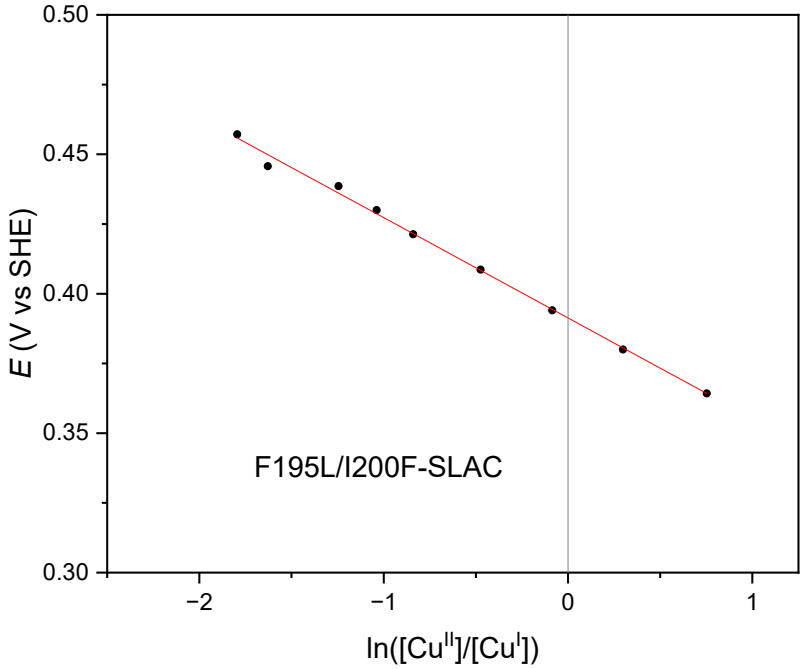

Figure S9. Redox titration of F195L/I200F-SLAC in 50 mM MOPS 150 mM NaCl pH 7 buffer. (R^2 = 0.996)

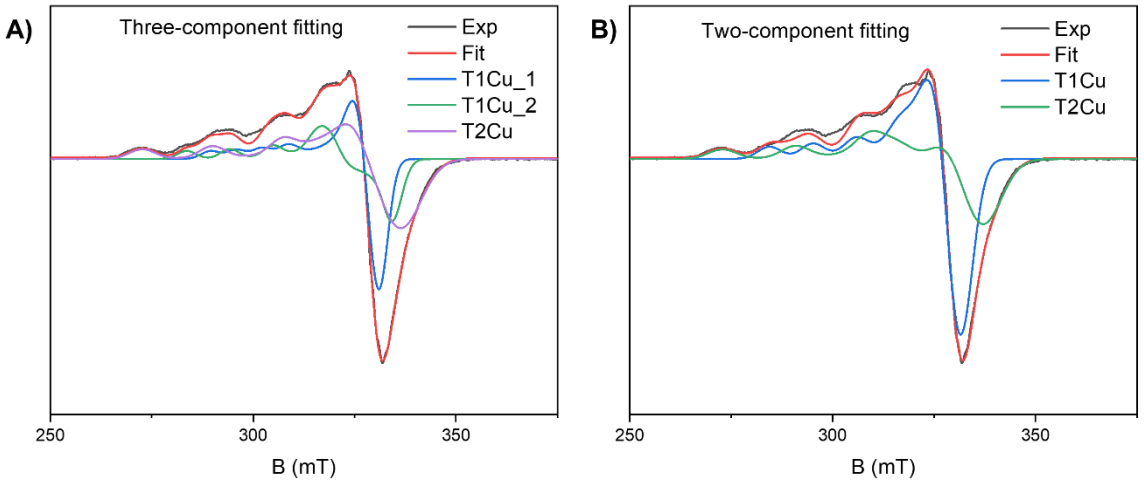

Figure S10. EPR spectrum fitting of LF-M298L-SLAC using A) three-component fitting and B) two-component fitting.

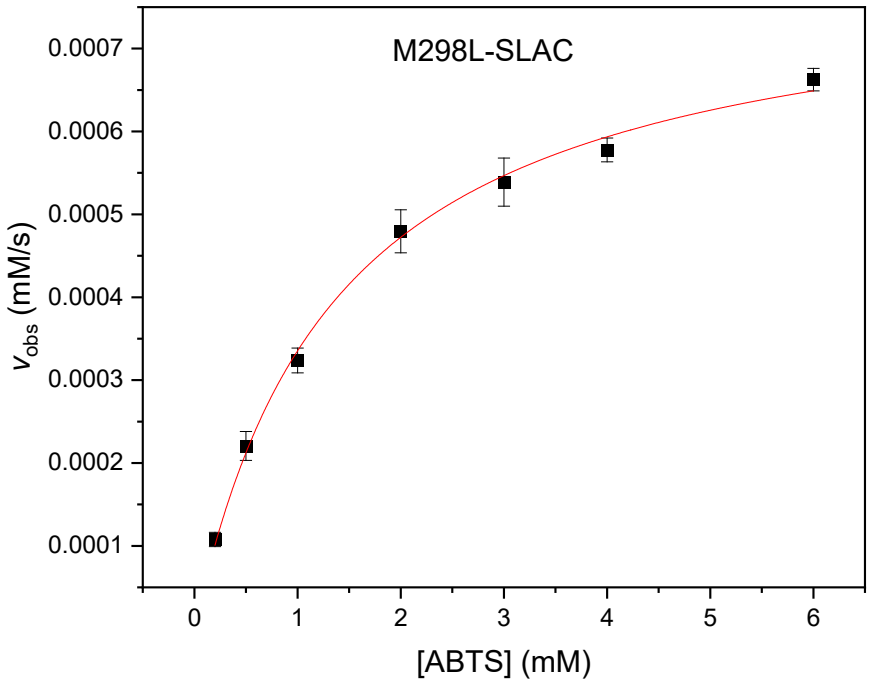

Figure S11. Michaelis-Menten plot for 5 µM M298L-SLAC using ABTS as substrate in 50 mM MOPS 150 mM NaCl pH 7 buffer.

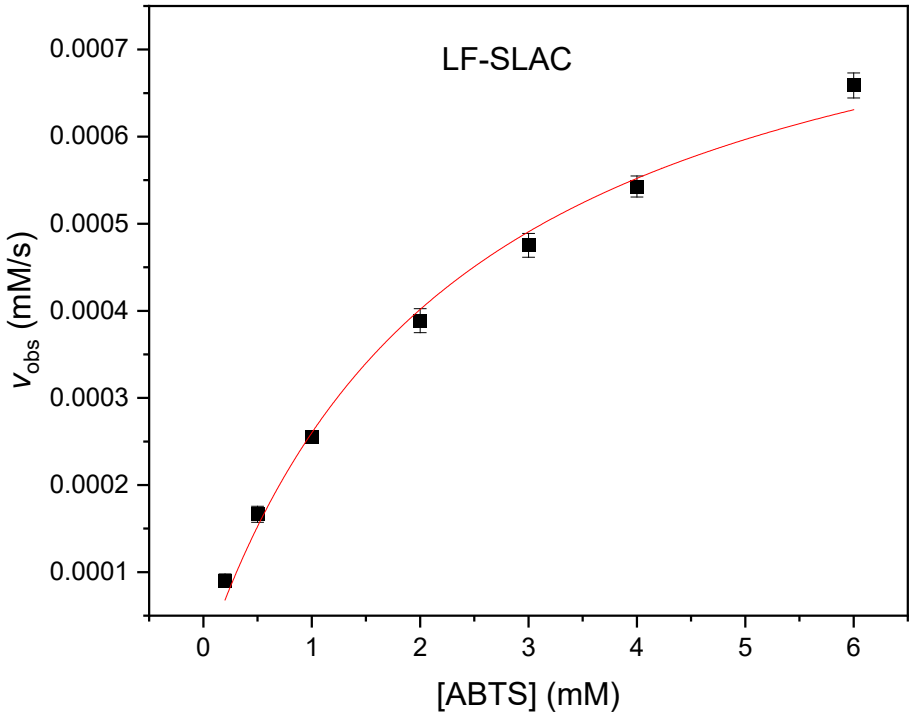

Figure S12. Michaelis-Menten plot for 1 µM LF-SLAC using ABTS as substrate in 50 mM MOPS 150 mM NaCl pH 7 buffer.

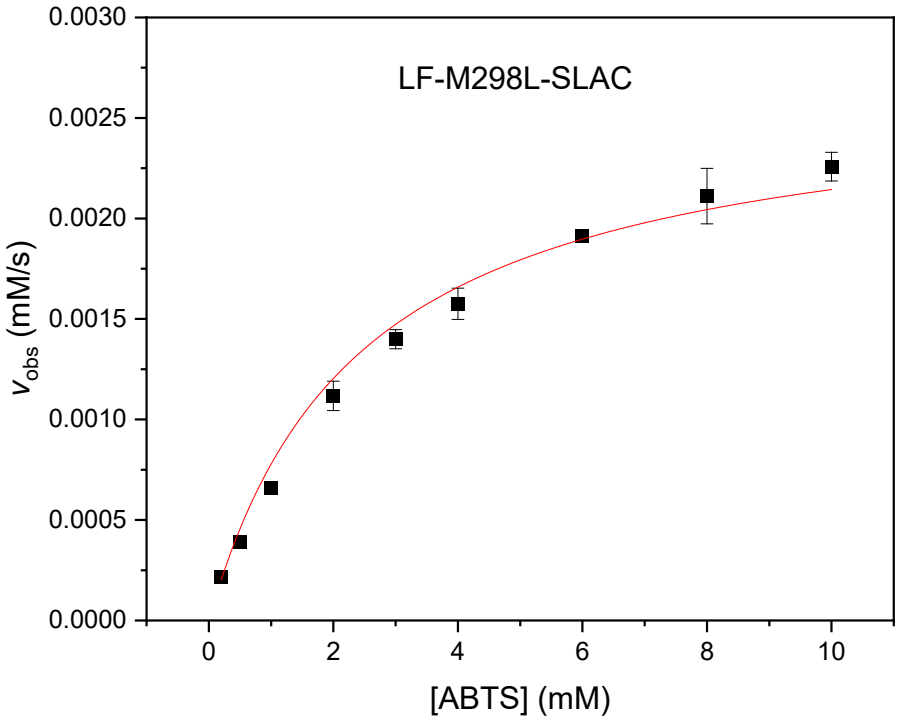

Figure S13. Michaelis-Menten plot for 1 µM LF-M298L-SLAC using ABTS as substrate in 50 mM MOPS 150 mM NaCl pH 7 buffer.

Table S1. EPR parameters of T2Cu for mutants involved in this study. All samples were measured in 50 mM MOPS 150 mM NaCl, pH 7 buffer.

		$g_{\perp}, g_{//}$	$A_{\perp}, A_{//}$ ($\times 10^{-4}$ cm^{-1})	Weight (%)
WT-SLAC[1]	T1Cu	2.043, 2.229	0.2, 67.0	50
	T2Cu	2.052, 2.259	40.0, 173.3	50
M298L-SLAC	T1Cu	2.051, 2.249	0.3, 78.1	50
	T2Cu	2.056, 2.258	33.4, 168.4	50
LF-SLAC	T1Cu	2.045, 2.217	0.2, 70.3	50
	T2Cu	2.055, 2.257	33.1, 182.0	50
LF-M298L-SLAC	T1Cu species **1**	2.047, 2.251	1.2, 65.7	25
	T1Cu species **2**	2.055, 2.247	35.9, 109.1	25
	T2Cu	2.048, 2.252	24.5, 178.7	50

Table S2. 2,2'-biquinoline assay results for all mutants.

Mutant	Total Cu / T1Cu
M298L-SLAC	4.3 ± 0.5
LF-SLAC	3.9 ± 0.2
LF-M298L-SLAC	4.5 ± 0.3

Table S3. Crystallography statistics of M298L-SLAC. Statistics for the highest resolution shell are shown in parentheses.

	M298L-SLAC
Wavelength (Å)	1.032995
Resolution range	44.31 - 2.6 (2.693 - 2.6)
Space group	P 43 3 2
Unit cell (Å, °)	177.228 177.228 177.228 90 90 90
Total reflections	1209476 (121150)
Unique reflections	29840 (2930)
Multiplicity	40.5 (41.3)
Completeness (%)	99.95 (100.00)
Mean I/sigma(I)	13.83 (1.76)
R-merge	0.2881 (2.191)
R-meas	0.2917 (2.218)
R-pim	0.04556 (0.3435)
CC1/2	0.997 (0.773)
CC*	0.999 (0.934)
Reflections used in refinement	29837 (2930)
Reflections used for R-free	1449 (151)
R-work	0.1833 (0.2731)
R-free	0.2001 (0.3187)
Number of non-hydrogen atoms	2358
macromolecules	2170
ligands	31
solvent	157
Protein residues	282
RMS(bonds) (Å)	0.002
RMS(angles) (°)	0.49
Ramachandran favored (%)	97.83
Ramachandran allowed (%)	2.17
Ramachandran outliers (%)	0
Rotamer outliers (%)	0.45
Clashscore	3.5
Average B-factor (Å^2)	47.9
Macromolecules (Å^2)	47.1
Copper (Å^2)	46.7
Solvent (Å^2)	55.3

Table S4. Crystallography statistics of F195L/I200F/M298L-SLAC. Statistics for the highest resolution shell are shown in parentheses.

	F195L/I200F/M298L-SLAC
Wavelength (Å)	1.000006
Resolution range	79.53 - 2.64 (2.734 - 2.64)
Space group	P 43 3 2
Unit cell (Å, °)	177.832 177.832 177.832 90 90 90
Total reflections	1138187 (111632)
Unique reflections	28814 (2808)
Multiplicity	39.5 (39.8)
Completeness (%)	99.96 (99.93)
Mean I/sigma(I)	16.58 (1.69)
R-merge	0.2716 (2.903)
R-meas	0.2751 (2.94)
R-pim	0.04341 (0.4634)
CC1/2	0.998 (0.849)
CC*	1 (0.958)
Reflections used in refinement	28805 (2806)
Reflections used for R-free	1506 (136)
R-work	0.1835 (0.2682)
R-free	0.2054 (0.2837)
Number of non-hydrogen atoms	2366
macromolecules	2186
ligands	31
solvent	149
Protein residues	282
RMS(bonds) (Å)	0.002
RMS(angles) (°)	0.48
Ramachandran favored (%)	97.83
Ramachandran allowed (%)	2.17
Ramachandran outliers (%)	0
Rotamer outliers (%)	1.33
Clashscore	3.94
Average B-factor (Å^2)	52.9
Macromolecules (Å^2)	52.0
Copper (Å^2)	57.3
Solvent (Å^2)	60.8

References

1 J. Wang, A. C. Vilbert, C. Cui, E. N. Mirts, L. H. Williams, W. Kim, J. Y. Zhang and Y. Lu, *Angew. Chem. Int. Ed.*, 2023, **62**, e202314019.
2 G. Felsenfeld, *Arch. Biochem. Biophys.*, 1960, **87**, 247–251.
3 S. Stoll and A. Schweiger, *J. Magn. Reson.*, 2006, **178**, 42–55.
4 M. C. Machczynski, E. Vijgenboom, B. Samyn and G. W. Canters, *Protein Sci.*, 2004, **13**, 2388–2397.
5 G. Winter, *J. Appl. Crystallogr.*, 2010, **43**, 186–190.
6 G. Winter, D. G. Waterman, J. M. Parkhurst, A. S. Brewster, R. J. Gildea, M. Gerstel, L. Fuentes-Montero, M. Vollmar, T. Michels-Clark, I. D. Young, N. K. Sauter and G. Evans, *Acta Crystallogr. Sect. Struct. Biol.*, 2018, **74**, 85–97.
7 M. D. Winn, C. C. Ballard, K. D. Cowtan, E. J. Dodson, P. Emsley, P. R. Evans, R. M. Keegan, E. B. Krissinel, A. G. W. Leslie, A. McCoy, S. J. McNicholas, G. N. Murshudov, N. S. Pannu, E. A. Potterton, H. R. Powell, R. J. Read, A. Vagin and K. S. Wilson, *Acta Crystallogr. D Biol. Crystallogr.*, 2011, **67**, 235–242.
8 L. Potterton, J. Agirre, C. Ballard, K. Cowtan, E. Dodson, P. R. Evans, H. T. Jenkins, R. Keegan, E. Krissinel, K. Stevenson, A. Lebedev, S. J. McNicholas, R. A. Nicholls, M. Noble, N. S. Pannu, C. Roth, G. Sheldrick, P. Skubak, J. Turkenburg, V. Uski, F. von Delft, D. Waterman, K. Wilson, M. Winn and M. Wojdyr, *Acta Crystallogr. Sect. Struct. Biol.*, 2018, **74**, 68–84.
9 P. D. Adams, P. V. Afonine, G. Bunkóczi, V. B. Chen, I. W. Davis, N. Echols, J. J. Headd, L.-W. Hung, G. J. Kapral, R. W. Grosse-Kunstleve, A. J. McCoy, N. W. Moriarty, R. Oeffner, R. J. Read, D. C. Richardson, J. S. Richardson, T. C. Terwilliger and P. H. Zwart, *Acta Crystallogr. D Biol. Crystallogr.*, 2010, **66**, 213–221.
10 A. J. McCoy, R. W. Grosse-Kunstleve, P. D. Adams, M. D. Winn, L. C. Storoni and R. J. Read, *J. Appl. Crystallogr.*, 2007, **40**, 658–674.
11 P. Emsley, B. Lohkamp, W. G. Scott and K. Cowtan, *Acta Crystallogr. D Biol. Crystallogr.*, 2010, **66**, 486–501.
12 V. B. Chen, W. B. Arendall, J. J. Headd, D. A. Keedy, R. M. Immormino, G. J. Kapral, L. W. Murray, J. S. Richardson and D. C. Richardson, *Acta Crystallogr. D Biol. Crystallogr.*, 2010, **66**, 12–21.
13 Schrodinger, 2023.
14 P. Eastman, R. Galvelis, R. P. Peláez, C. R. A. Abreu, S. E. Farr, E. Gallicchio, A. Gorenko, M. M. Henry, F. Hu, J. Huang, A. Krämer, J. Michel, J. A. Mitchell, V. S. Pande, J. P. Rodrigues, J. Rodriguez-Guerra, A. C. Simmonett, S. Singh, J. Swails, P. Turner, Y. Wang, I. Zhang, J. D. Chodera, G. De Fabritiis and T. E. Markland, *J. Phys. Chem. B*, 2024, **128**, 109–116.
15 J. Huang and A. D. MacKerell Jr, *J. Comput. Chem.*, 2013, **34**, 2135–2145.
16 N. M. Marshall, D. K. Garner, T. D. Wilson, Y.-G. Gao, H. Robinson, M. J. Nilges and Y. Lu, *Nature*, 2009, **462**, 113–116.
17 A. D. MacKerell, D. Bashford, M. Bellott, R. L. Dunbrack, J. D. Evanseck, M. J. Field, S. Fischer, J. Gao, H. Guo, S. Ha, D. Joseph-McCarthy, L. Kuchnir, K. Kuczera, F. T. K. Lau, C. Mattos, S. Michnick, T. Ngo, D. T. Nguyen, B. Prodhom, W. E. Reiher, B. Roux, M. Schlenkrich, J. C. Smith, R. Stote, J. Straub, M. Watanabe, J. Wiórkiewicz-Kuczera, D. Yin and M. Karplus, *J. Phys. Chem. B*, 1998, **102**, 3586–3616.
18 T. Skálová, J. Dohnálek, L. H. Østergaard, P. R. Østergaard, P. Kolenko, J. Dušková, A. Štěpánková and J. Hašek, *J. Mol. Biol.*, 2009, **385**, 1165–1178.
19 H. Nar, A. Messerschmidt, R. Huber, M. van de Kamp and G. W. Canters, *J. Mol. Biol.*, 1991, **221**, 765–772.